1
2

Practice-oriented buildability criteria for developing 3D-printable concretes in the context of digital construction

3

Venkatesh Naidu NERELLA[a]*, Martin KRAUSE[b], Viktor MECHTCHERINE[a]

4
5
6
7
8

[a]*Institute of Construction Materials, Von-Mieses-Bau, 3 O.G., Georg-Schumann-Str. 07, Technische Universität Dresden, 01087 Dresden, Germany*
[b]*Institute of Construction Management, Nürnberger Ei, 4. O.G., Nürnberger Straße 31A, Technische Universität Dresden, Dresden, Germany*
* *corresponding author, tel.: +49 351 463 35922, fax: +49 351463 37268, e-mail: nerella@msx.tu-dresden.de*

9

Abstract

10
11
12
13
14
15
16
17
18
19
20
21

Buildability, i.e. the ability of a deposited material bulk to retain its dimmensions under increasing load, is an inherent prerequisite for formwork-free digital construction (DC). Since DC processes are relatively new, no standard methods of characterization are available yet. The paper at hand presents practice-oriented buildabilty criteria by taking various process parameters and construction costs into consideration. In doing so, direct links between laboratory buildability tests and target applications are established. A systematic basis for calculating the time interval (TI) to be followed during laboratory testing is proposed for the full-width printing (FWP) and filament printing (FP) processes. The proposed approach is validated by applying it to a high-strength, printable, fine-grained concrete. Comparative analyses of FWP and FP revealed that to test the buildability of a material for FP processes, higher velocities of the printhead should be established for laboratory tests in comparison to those needed for FWP process, providing for equal construction rates.

22

Highlights:

23   1. Practice-oriented criteria for characterizing buildability are proposed.
24   2. The applicability of the model in quantifying the economic viability of 3D-printing is
25   demonstrated.
26   3. Specimen height and time interval are specified as parameters for buildability tests on
27   printable concretes.
28   4. Proposed buildability criteria are validated by tests on a printable concrete.
29   5. Variations regarding buildability test specifications for full-width and filament printing
30   techniques are described.

31   **Keywords**: Digital Construction; 3D-concrete-printing; buildabiltiy, additive manufacturing.

32   ## 1. Introduction and definitions

33   ### 1.1 Digital construction and requirements for fresh concrete

34
35
36
37
38
39

The processing of cementitious materials is the technological core of modern construction. In recent years numerous new construction techniques based on digitalization and automation have been developed; see e.g. [1–6]. These modern construction processes can be referred to with the generic process title *Digital Construction (DC),* which denotes automated additive (or generative) construction with cementitious materials. DC opens a multitude of opportunities and technological advancements:

40   • no need for formwork, enabling high geometric flexibility [6,7],

41   • additional functionalities [1,2,6],

42   • considerable reductions in time and cost [5,8],

43   • low dependency on skilled labor, *etc*.

44   However, the major significance and revolutionary potential of DC reveal themselves in the context
45   of Construction Industry 4.0 since it represents a logical, decisive step arising from the already
46   well-developed tools of digital design and planning (CAD, BIM, *etc*.) towards digital
47   manufacturing, thus making construction a fully digitalized, seamless process.

48   Two common digital construction techniques are selective material deposition by extrusion and
49   selective binding. The working principles and details of these two approaches are described in more
50   detail in, for example, [3,5], while Figure 1 presents examples of structures produced using these
51   techniques. When it comes to large-scale and on-site applications, extrusion-based techniques
52   appear more suitable; see Figure 1a. The dimensions of the printing device for selective binding
53   techniques must be bigger than those of the target structure [3,5,9]. This is not the case for many
54   extrusion-based DC technologies, as the examples of CONPrint3D [5] and Apis Cor [10]
55   demonstrate. Furthermore, in the case of selective material deposition by extrusion, material is
56   delivered only where it is needed permanently and should, therefore, be sufficiently "buildable".
57   In contrast, in selective binding techniques the support material surrounding the material to be
58   bonded is crucial to keeping its shape while it is still in plastic state. The need for support material
59   has both positive and negative consequences: structures of any geometrical shape can be produced
60   (positive); see Figure 1b, but all the non-bonded material must eventually be removed (negative).
61   Thus, at this stage the practical application of selective binding techniques seems to be feasible for
62   off-site production of complex elements having relatively small dimensions only. This is one
63   reason why this article focuses exclusively on extrusion-based techniques. Another reason is that
64   due to the mandatory presence of support material, buildability is not really a challenge in the
65   context of selective binding technology.

a)   b)

66   *Figure 1. Examples of digital construction approaches: a) structural elements produced on-site using selective*
67   *material deposition by extrusion [4], b) complex structure of Digital Grotesque II produced in a stationary 3D-*
68   *printer using selective binding technique [11]*

69   Based on layering technique, extrusion-based DC processes can be classified as full-width printing
70   (FWP) and filament printing (FP). In FWP the breadth of the extrudate is equal to that of the target

71   element, as in CONPrint3D; see Figure 2a. In case of FP the breadth of the extrudate is many times
72   smaller than the breadth of the target element, as in Contour Crafting [1,2,4,12,13] (Figure 2b) or
73   even more pronounced in fine filament approach called Concrete Printing [2,14,15]; see Figure 2c.
74   Consequently, a cross-section of FP elements consists of outer layers (shell/mold) and inner layers
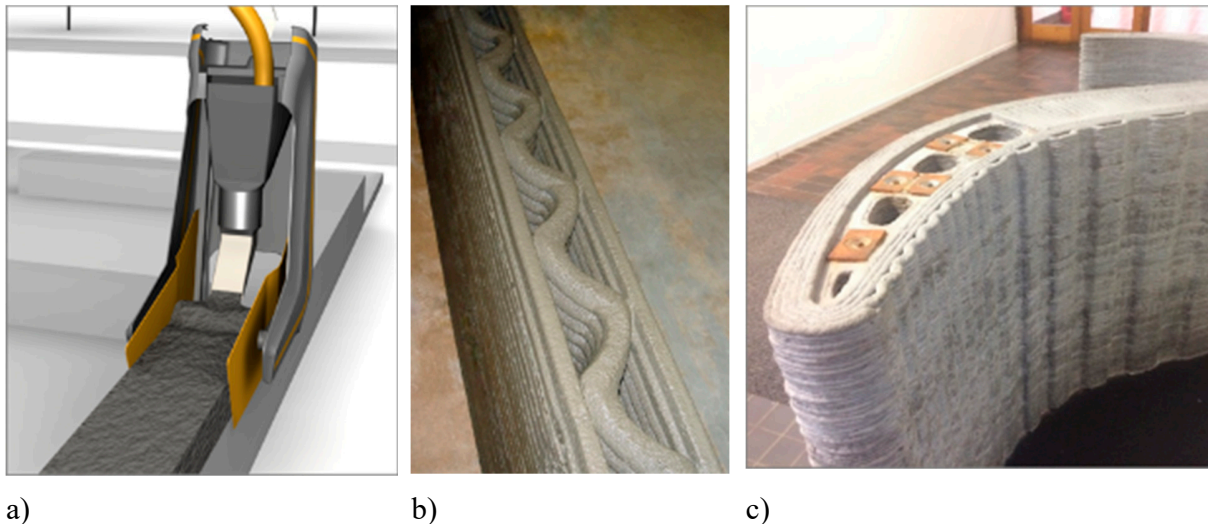75   or fillings.

a)   b)   c)

76   **Figure 2.** *a) CONPrint3D technology as example of full-width printing [courtesy: Chair of Construction Machines,*
77   *TU Dresden], b) Contour Crafting as example of filament printing [courtesy: Contour Crafting], c) Wonder Bench*
78   *at Loughborough University as example of fine filament printing (photo by V. Mechtcherine)*

79   In terms of engineering properties, the primary requirements of cementitious materials for selective
80   material deposition by extrusion are: 1) pumpability, 2) extrudability, and 3) buildability; see also
81   Figure 3. Adequate pumpability should ensure the uninterrupted transportation of fresh concrete
82   and depends on, among other parameters, the plastic viscosity of the concrete, or rather the
83   formation of a lubricating layer [16–18]) in the first place. Extrudability refers to the ease of
84   continuously extruding a material at a given flow rate; it depends on the rheological properties of
85   the fresh concrete and the geometrical configuration of the extruder, or printhead. This being said,
86   buildability, the term and the central subject of this article, is defined as the ability of an extruded
87   material to retain its geometry (shape and size) under sustained and increasing loads. The
88   explanation of this definition follows in Section 1.2.

89   As pointed out in [5], DC is a process of many dualities, e.g. the duality of pumpability and
90   buildability since rheological properties favorable for each of these two processes differ markedly,
91   or the duality arising while determining the 'rate of printing', incl. economic efficiency, possible
92   formation of "cold joints", *etc*. From a scientific perspective the rheological properties of fresh
93   cementitious material are the most crucial aspect of DC, since they affect not only the process
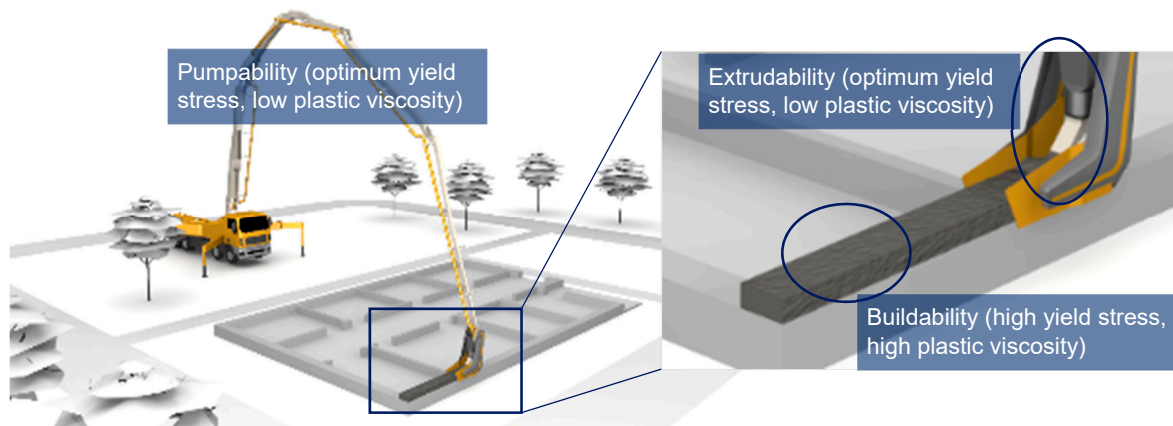94   parameters but also the properties of the final product.

95

Figure 3. Illustration of key properties for printable concrete on example of CONPrint3D technology (base sketches are of courtesy: Chair of Construction Machines, TU Dresden).

To fulfil the main requirements of extrusion-based DC, cementitious material should be thixotropic, quick setting, quickly hydrating to develop strength very early, and densely packed, and it should possess well controlled rheological properties such as yield stress and plastic viscosity, possibly controllable through internal or external triggers [19]. While this general approach is widely understood, many essential aspects are still under research. The open questions include the systematic choice of rheological parameters and identification of their threshold values. Most importantly, validated experimental methods are necessary to characterize and ensure the desired material properties. In their work in this connection the authors address the question of how one of the primary engineering properties of cementitious materials for DC, namely buildability, can be systematically characterized. Specifically addressed are the questions of what a representative piece of wall is, i.e. height, breadth to be tested in lab-scale buildability tests, and what are the time intervals to be tested in order to call a material printable are addressed.

1.2 Buildability requirements and the problem definition

Buildability is the ability of extruded material to retain its geometric dimensions, both shape and size, under sustained or increasing loads. It is a complex, process-specific property which depends not only on material composition, but on process parameters such as layer geometry as well; cf. Figure 2. If buildability, printing rate, printing pattern, and other related aspects are not in harmony, the 3D-printed structure will collapse; see Figure 4b. Buildability depends on, but is not identical to, the structural build-up of cement-based materials, and this dependence is not exclusive.

From a practical perspective, there are three primary parameters defining any buildability criteria when applied in laboratory investigations for material characterization: 1) the height of the wall to be printed, 2) the height of each layer or the total number of layers to be printed, and 3) the time interval (TI) between subsequent layers.

Since many of the properties required for 3D-printable concretes need a "perfect" balance, it is essential to consider target application at all stages of material development. The buildability-defining parameters mentioned above must be carefully determined, considering various theoretical and practical aspects and then applying them in testing the applicability of particular

125 mixtures for target DC. 3D-printed elements should have consistent and continuous layer geometry
126 over the entire structure. Figure 4 shows an example of printed specimens with varying numbers
127 of layers and buildabiltiy. It is often appealing to print 10, 20 or as many layers as possible and
128 then 'designate' the material as buildable. This trivial approach neither links the material's fresh
129 properties to the target geometry nor does it consider the economic viability of the target
130 application. While such an approach is still useful for relative comparison of various compositions,
131 printing an arbitrary number of layers with an arbitrary time interval TI is not a reliable method in
132 characterizing buildability. Flowable concrete with low static yield stress, extruded to wide, but
133 thin layers using a long $TI,$ will likely sustain deposition of a higher number of layers in comparison
134 to a less flowable concrete but deposited with a much higher aspect ratio $\alpha_{L,app}$ of individual layers
135 and a short TI; see Section 2. Further relevant parameters are economic viability and durability of
136 the structure, both dependent on TI. Durability is a function of the quality of interlayer joints, which
137 very importantly depends on TI. Thus, for buildability it is crucial to determine one criterion or
138 several criteria based on the intended application and estimated process parameters.

139 In Section 2 previously proposed approaches to estimate buildability based on rheological
140 modelling are critically presented before our own practice-oriented criteria are introduced, which
141 define buildability in terms of target application and process parameters. The applicability of
142 proposed criterion is demonstrated on an example DC process in Section 3, deducing preferable
143 layer height and time interval needed as a basis for developing suitable concretes. Since buildability
144 requirements depend not only upon the target structure but also on the applied printing approach,
145 e.g. massive vs. 'hollow with sinusoidal cores' as seen in Figure 2, a corresponding comparative
146 analysis is presented in Section 4.

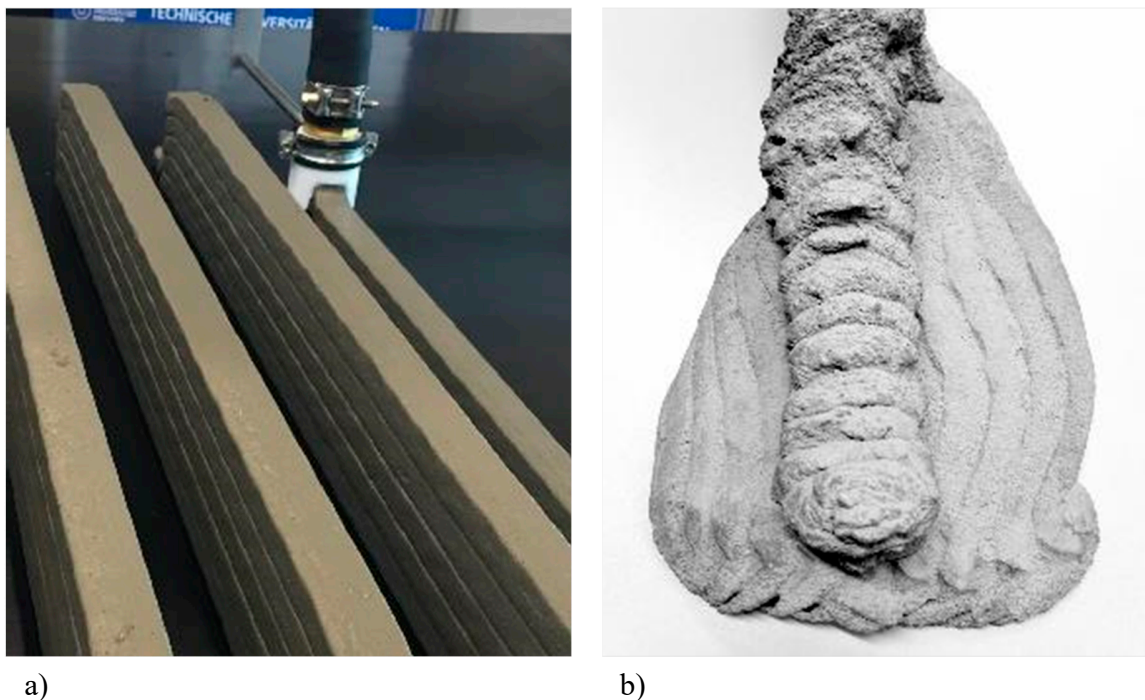a)   b)

147
148   ***Figure 4.*** *a) 3D-printed fine-grained concrete specimens (up to five printed layers are depicted here, time interval*
149   *was 30 s), b) a collapsed printed specimen with buildability deficiency.*

2. Buildability criteria considering target application

2.1 Previous approaches

Buildability criteria based on fundamental rheological properties, e.g. static yield stress, and the associated changes over time are still in their genesis; it will take some years until development and validation are complete. Generic rheological models which can consider various process techniques, the shape of the extrudate, and the effects of temperature and other surrounding conditions will take even longer to be formulated and proven. All that existing criteria can predict is whether a deposited material during a time of rest t_{rest} deforms or not. However, they do not consider the economic viability of the target application, meaning that even if a material is proven buildable as such at a particular printing rate, it is not known how the use of that particular material/printing rate influences the total economic viability of the target project. Hence, simple, practice-oriented, yet rational buildability-assurance criteria are necessary to accelerate the implementation of digital technologies in construction practice. One such approach is presented in the following sections.

In the limited literature on the subject of this article, three significant contributions can be identified [19–21]. In the first on-the-topic, commendable work, Perrot *et al.* [20] considered the following primary criterion: 'the flow resistance of a substrate-layer should always be higher than the vertical loads acting on top of it'. The researchers expressed the vertical loads in terms of printing speed and hydrostatic pressure of concrete using Eq. 1:

$$\sigma_v = \rho \cdot g \cdot R \cdot t \qquad\qquad Eq.\ 1$$

where ρ is the specific weight of concrete, g is the gravity constant, R is rate of construction, and t is the time of construction.

The flow resistance of the substrate-layer, expressed as time-dependent static yield stress is described by Eq. 2, Perrot's exponential evolution model for thixotropy [22]:

$$\sigma_c(t) = \tau_0(t) = \alpha_{geom}\left(\tau_{0,0} + A_{thix} \cdot t_c \left(e^{\frac{t_{rest}}{t_c}} - 1\right)\right) \qquad\qquad Eq.\ 2$$

where $\tau_{0,0}$ and $\tau_0(t)$ are static yield stresses of the material when resting time is *zero* and *t*, respectively; A_{thix} is the constant rate of increase in the static yield stress; t_c is a characteristic time after which yield stress evolution at rest becomes exponential; α_{geom} is a geometric factor which depends on the geometry of the deposited layer/printed element [20].

Alternatively, the resistance of a substrate-layer can be estimated using Roussel's linear evolution model for thixotropy [23]; see Eq. 3:

$$\sigma_c(t) = \tau_0(t) = \alpha_{geom}\left(\tau_{0,0} + A_{thix} \cdot t_c\right) \qquad\qquad Eq.\ 3$$

Applying buildability criteria according to Perrot *et al.* [20] (Eq. 1) for Eqs. 2 and 3, we obtain:

$$\rho \cdot g \cdot R \cdot t \leq \alpha_{geom}\left(\tau_{0,0} + A_{thix} \cdot t_c \left(e^{\frac{t_{rest}}{t_c}} - 1\right)\right) \qquad\qquad Eq.\ 4$$

$$\rho \cdot g \cdot R \cdot t \leq \alpha_{geom}\left(\tau_{0,0} + A_{thix} \cdot t_c\right) \qquad\qquad Eq.\ 5$$

185 Finally, a critical failure time t_f according to Perrot with Roussel' linear model [23] for thixotropy
186 is:

187 $$t_f = \frac{\tau_{0,0}}{\frac{\rho \cdot g \cdot R}{\alpha_{geom}} - A_{thix}}$$ *Eq. 6*

188 t_f predicts at what time after deposition the concrete specimen fails/fractures, if vertical load is
189 increased at rate R and the material initial yield stress $\tau_{0,0}$ is evolving linearly [23] with a slope
190 A_{thix}.

191 Similar to Perrot *et al.*, Wangler *et al.* [19] rely on the relationship of flow resistance of a substrate-
192 layer, expressed as static yield stress, to the vertical loads acting on top of it. Wangler's model for
193 minimum time to print a layer follows Von Miese's criteria and Roussel' linear model [23] for
194 structural build-up:

195 $$t_{h,min} = \frac{\rho \cdot g \cdot h}{\sqrt{3} \cdot A_{thix}}$$ *Eq. 7*

196 In other words, the minimum time $t_{h,min}$ for producing a layer can also be termed as the minimum
197 interval between two successive layers needed to ensure "buildability".

198 Even though both of these works above are outstanding contributions to the subject of this paper,
199 there are still a few challenges to be mastered before these criteria can become widely applicable.
200 For instance, the parameter α_{geom} is not generically defined yet. Perrot *et al.* [20] computed α_{geom}
201 from the squeeze flow theory of plastics [24,25]. Determining the structuration parameter A_{thix} is
202 also not a trivial task. Currently there are neither standard devices nor standard protocols for
203 characterizing A_{thix} of cementitious materials. Even using most modern rheometers different A_{thix}
204 values may be derived for the same material when different measuring protocols are employed.
205 This implies that for the same material, different critical failure time or minimum time intervals
206 can be computed using Eq. 6 and Eq. 7, respectively.

207 Furthermore, Eq. 6 and Eq. 7 are formulae for the onset of flow/deformation. This means that even
208 if all parameters, including α_{geom} and A_{thix}, are determined precisely, the primary calculation result
209 will be whether the material will deform or not. Such a prediction naturally underestimates the
210 ability of the material to withstand applied loads. In fact, in most practical cases a perfectly rigid
211 layer is not necessary; a layer which deforms within the tolerances allowed is acceptable. An
212 equilibrium reached after few millimeters of deformation is a common possibility as observed in
213 the experiments conducted by the authors and by many other researchers as well. For the target
214 application of the CONPrint3D technology – the construction of residential buildings in Germany
215 – the DIN 18202 "Tolerances in building construction – buildings" [26] specifies the permissible
216 dimensional tolerances and deviations including the specified requirements for the flatness of the
217 wall. When translated for digital construction, i.e. stacking the layers, the DIN 18202 specifications
218 imply that deviations of up to 5 mm between each layer are permissible. Still further, the permitted
219 dimensional deviations from the floor plan depend on the length of the wall. For example,
220 deviations of 12 mm are permitted for a 3 m long wall. These observations, combined with
221 advantages of better inter-layer bonds and pumpability, add strength to the argument for giving

222 priority to a material which deforms within an allowed limit, as opposed to a perfectly rigid
223 material.

224 More recently, Wolfs *et al.* [21] developed and validated a numerical model for predicting the
225 failure of 3D-printed concrete. Attributing early strength (0 to 90 min) of printed concrete to
226 "combined inter particle friction and cohesion", they have adopted Mohr-Coulomb failure criteria,
227 also considering time-dependency [21]. This model does not require measurement of A_{thix} and
228 computation of α_{geom} as in the above-described rheology-based approaches, and the experimental
229 validation of the numerical model showed good qualitative and acceptable quantitative
230 correlations. This approach, however, requires extensive experimental studies and, similar to
231 rheology-based approaches, high precision in execution is needed. In addition, the approach did
232 not address the economic viability of the target application. A simple, practice-oriented criterion
233 for buildability tests has yet to be reported. Note that an extensive review of buildability testing
234 approaches is not the scope of the paper at hand.

235 Process-induced changes in rheological properties is another crucial subject. For example, in the
236 case of pumping SCC, differences in values of yield stress and plastic viscosity were recorded
237 before and after pumping [28]. The variation in rheological properties may result from the "higher
238 shear rates leading to the dispersion of cement particles and depending on available residual
239 superplasticizer in the mixing water" [28]. Additional data on losses in slump, changes of air-void
240 systems, influence of pressure on rheological properties can be found in [29,30]. When it comes to
241 3D-printing based on extrusion on a laboratory scale, even though the material is generally not
242 pumped over large distances, it undergoes high shear rates and is subjected to high pressure in the
243 extruder. Therefore, the exact rheological state of the extrudate may vary depending on the specific
244 extruder and printing-circuit (mixing-transporting-extruding). If large-scale, on-site applications
245 are realized, a pronounced influence of process/pumping on the material rheological state is to be
246 expected. Since rheological properties are usually measured on material taken immediately after
247 mixing, variations of these off-line measured properties in comparison to the actual extrudate
248 rheological properties are inherent. This, however, can be solved by carrying out extensive
249 experimental studies and by the fitting of theoretically predicted "buildability" and experimentally
250 observed "buildability". To the best of the authors' knowledge, no such studies have been reported
251 yet.

2.2 Suggested buildability criteria

253 The first step in the proposed approach is to identify and define the target application. Based on
254 the building design and project planning, a detailed printing scenario must be established. This task
255 is normally seen as part of the 'design and process' aspect of DC work flow. Generally it involves
256 'slicing' the 3D geometry, identifying optimum travel route of the printhead, and determining layer
257 breadth, height, and contours. In the case of massive full-width printing (FWP) such as with the
258 CONPrint3D approach [5], layer breadth is equal to final breadth of the wall to be printed; see
259 Figure 3. The criteria presented below are proposed for full-width layer printing. Criteria for
260 filament printing such as the case with Contour Crafting [1] are addressed in Section 4; see Figure
261 2b.

262   For the convenience of further discussion in this article, authors define various relevant aspect
263   ratios as listed in Table 1.

264   **Table 1.** Aspect ratios of various elements produced by means of digital construction

Element	Aspect ratio	
	Notation	Definition
Target wall	α_{app}	Ratio of target wall's height H_{app} to breadth B_{app}
Experimental specimen	α_{exp}	Ratio of H_{exp} to breadth B_{exp} of the wall produced in lab experiment
Target layer	$\alpha_{L,app}$	Ratio of height $H_{L,app}$ to breadth $B_{L,app}$ of one layer in the target wall
Experimental layer	$\alpha_{L,exp}$	Ratio of height $H_{L,exp}$ to breadth $B_{L,exp}$ of one layer in the wall produced in lab experiment

265

266   If the height and breadth of the wall to be printed (part of the target structure) are H_{app} and B_{app},
267   respectively, then the aspect ratio of the continuously produced "target" element whose buildability
268   has to be ensured can be expressed by Eq. 8:

269    $\alpha_{app} = \frac{H_{app}}{B_{app}}$ *Eq. 8*

270   Naturally, the most straightforward but often economically unfeasible manner in verifying
271   buildability is to produce a full-scale structure of the targeted application. Alternatively,
272   buildability can be tested by producing a scaled-down version of the target structure in a laboratory
273   with an appropriate 3D-printing device. In this case printing an arbitrary number of layers with an
274   even so arbitrary time interval *TI* will, however, not prove a material buildable; see also Section
275   1.2. Thus, the authors propose calculating the minimum height $H_{min,exp}$ of the wall to be tested in
276   the laboratory, using the breadth of the layers printed in laboratory experiments B_{exp} and target
277   structure's aspect ratio α_{app} (Eq. 8) as:

278    $H_{min,exp} = B_{exp} \cdot \alpha_{app}$ *Eq. 9*

279   If the height of a single layer printed in laboratory experiments is $h_{layer,exp}$

280   the total number of layers to be printed

281    $n_{layers} = \frac{H_{min,exp}}{h_{layer,exp}}$ *Eq. 10*

282   Combining, Eq. 9 and Eq. 10 give:

283    $n_{layers} = \frac{\alpha_{app} \cdot B_{exp}}{h_{layer,exp}}$ *Eq. 11*

284   When downscaling the wall geometry to a laboratory specimen, the limits given by each particular
285   concrete composition must be considered. Specifically, the maximum aggregate of mixtures poses
286   a requirement of minimum breadth and height of each single layer. Choosing the minimum
287   dimension of layer cross-section to be the trifold of the maximum aggregate size seems to be

288   adequate here. Such a ratio ensures that no pronounced wall effects occur so that the features of
289   the material do not change and the material can be well extruded. Further comments on
290   downscaling, including possible changes in maximum aggregate size, follow in Section 2.3.

291   The next open question revolves around determining the time interval between layers *TI*, which
292   depends on the rate of printing. Rate of printing is a very crucial parameter for formwork-free
293   construction with time-dependent materials such as concrete. If the rate of printing is too high, the
294   printed concrete may not have sufficient time for structural build-up [31] and hence cannot retain
295   its shape and size. If rate of printing is too low, total construction time and costs might become
296   unfeasible. In addition, lower construction rates give rise to so-called "cold joints", i.e. weak
297   interface bonds between the layers. This leads to the deterioration of both mechanical properties
298   and durability. The time interval *TI* to be followed in laboratory tests can be deduced directly from
299   the target process parameters. The total travel length *L* of the printhead can be determined from the
300   layout/floorplan of the target application; see Figure 5. With an average (horizontal) printing
301   velocity of V_{DC}, the minimum time interval between two layers can be expressed as:

302    $TI_{min} = L / V_{DC}$ *Eq. 12*

303   In the first approximation V_{DC} is assumed constant, not accounting for a) the acceleration and
304   deceleration at the beginning and the end of printing one layer, respectively, and b) velocity
305   variations when printing corners. For $TI > L/V_{DC}$, the printing process has to be halted, e.g. to
306   account for possibly insufficient buildability of the applied material, thus leading to longer
307   construction times and losses in efficiency. For $TI < L/V_{DC}$ concrete buildability is over-engineered,
308   i.e. more than necessary, which may affect the interlayer bond negatively, but also poses greater
309   challenges in meeting the requirements of pumpability and extrudability. While defining *TI,* the
310   economic viability of the target application/project must be considered as well. The corresponding
311   process term, the average velocity V_{DC}, is already addressed in Eq. 12. It is worthy of note that for
312   a wall of given gross dimensions, the time interval *TI* will be in the case of FP approaches higher
313   than that for FWP approaches due to longer total travel length of the printhead. This aspect is
314   elaborated in Section 4. For any DC approach to be economically viable, the following condition
315   according to Eq. 13 must be fulfilled:

316    $Costs_{DC} \leq Costs_{CC}$ *Eq. 13*

317   where, $Costs_{DC}$ and $Costs_{CC}$ are the respective total construction costs in the case of the DC
318   approach chosen and in the case of current corresponding conventional construction (CC)
319   approach, respectively. Authors have identified, as an example, replacing masonry structures for
320   residential buildings as the strategic objective for CONPrint3D [5,8]. Therefore, in this case
321    $Costs_{CC}$ are the current total construction costs for masonry in a unit residential building.

322   Expressing the costs of machine and labor as cost per unit time and material costs as cost per unit
323   volume, the total costs can be estimated by using Eq. 14:

324    $(McCo_{DC} + LaCo_{DC}) \cdot t_{DC} + MtCo_{DC} \cdot vol_{DC} + AdCo_{DC} \leq (McCo_{CC} + LaCo_{CC}) \cdot t_{CC} + MtCo_{CC} \cdot vol_{cc}$ *Eq. 14*

325   where, $McCo_{DC}$, $LaCo_{DC}$ and $McCo_{CC}$, $LaCo_{CC}$ are the machinery/equipment costs and labor costs
326   for DC and CC, respectively; $MtCo_{DC}$, $MtCo_{CC}$ are material costs for DC and CC, respectively;

327 $AdCo_{DC}$ are additional costs added only for DC. Additional costs include, among others, costs for
328 concrete curing (more elaborate than usual), additional testing and consulting fees that may be
329 necessary in the case of DC. t_{DC} and t_{CC} are the time needed for constructing the target structure
330 in case of DC and CC, respectively, while vol_{dc} and vol_{cc} are the total volumes of material used in
331 case of DC and CC, respectively.

332 Expressing time in terms of average velocity in the case of DC and inversed construction rate RI
333 (unit: h/m^2) in the case of CC, we obtain:

334 $(McCo_{DC} + LcCo_{DC}) \cdot \frac{L_t}{V_{DC}} + MtCo_{DC} \cdot vol_{DC} + AdCo_{DC} \leq (McCo_{CC} + LaCo_{CC}) \cdot (RI \cdot surface\ area) +$

335 $MtCo_{CC} \cdot vol_{CC}$ *Eq. 15*

336 where *surface area* is the total "one-side" surface area of the element being constructed; L_t is the
337 total travel length of the printhead, which is assumed to be equal to the travel length for a single
338 layer L multiplied by the total number of layers n_{layers}. The traversing of the printhead without
339 printing, for example, to move to a new printing position are not considered here as they are very
340 specific to the target application and the related process parameters. Nevertheless, these can be
341 added to the L_t if known.

342 Additional costs $AdCo_{DC}$ in the case of CONPritn3D are assumed to be a lump sum amounting to
343 10 % of the total construction costs.

344 Rearranging Eq. 15, Eq. 16 for the minimum average printhead velocity for an economically viable
345 DC application can be obtained:

346 $V_{DC,min} \geq \frac{(McCo_{DC} + LaCo_{DC}) \cdot L_t}{0.\overline{90} \cdot ((McCo_{CC} + LaCo_{CC}) \cdot (RI \cdot surface\ area) + MtCo_{CC} \cdot vol_{CC}) - (MtCo_{DC}) \cdot vol_{DC}}$ *Eq. 16*

347 Since it is known that:

348 • L_t is equal to the length of the layer multiplied by the total number of layers n_{layers},

349 • *surface area* is equal to the length of the layer multiplied by the height of the wall, and

350 • total material volume is the length multiplied by the height and breadth of the walls,

351 Eq. 16 can be transformed to Eq. 17:

352 $V_{DC,min} \geq \frac{(McCo_{DC} + LaCo_{DC}) \cdot n_{layers}}{0.\overline{90} \cdot ((McCo_{CC} + LaCo_{CC}) \cdot (RI \cdot H_{app}) + MtCo_{CC} \cdot H_{cc} \cdot B_{cc}) - MtCo_{DC} \cdot H_{DC} \cdot B_{CC}}$ *Eq. 17*

353 where H_{CC}, B_{CC}, H_{DC}, B_{DC} are the height and breadth of the walls in case of CC and DC,
354 respectively. While $H_{CC} = H_{DC}$ is chosen here for ease of comparison, the breadth of the layers
355 produced in DC can be smaller than that of CC. Since materials used for DC applications are often
356 superior to masonry in terms of mechanical performance, thinner walls produced using DC can
357 meet the same design specifications as thicker walls produced using CC. Eqs. 16 and 17 can be
358 adapted also to other DC applications to compute a minimum average printhead velocity that
359 should be attained to make the DC application economically viable with respect to the fabrication
360 process as such. Certainly there are also other factors which may influence the economic feasibility
361 to a great extent. Thus, in general the entire process from planning to actual construction should be
362 evaluated. Specifically, the smooth transition from digital planning to digital fabrication seems to
363 bring with it great technical and economic potential.

2.3 Additional comments

The proposed approach assumes that material behavior tested on the "down-scaled specimens under laboratory conditions (lab-tests)" is representative of the material behavior in "full-scale structure in real application (full-scale)". In reality differences in material behavior as among the lab-tests and as experienced full-scale may arise, e.g. due to variation in the quality of extrusion/compaction (process-induced changes) or in the evaporation rate related to the volume of printed element.

Here it is important to emphasize that the challenge posed by some differences in lab experiments and full-scale applications is a universal issue which is not particular to buildability tests or DC in general. Taken broadly, such issues can only be resolved by full-scale tests and direct comparison, followed by error-minimization measures. The approach proposed in this paper for laboratory tests already takes into account certain considerations in mimicking conditions under full-scale application:

    a) Tests are performed in-line, i.e. they are integrated in the 3D-printing process, as opposed to offline tests where material has to be collected separately and tested in a test device; thus, time-dependent influences are avoided and errors due to process induced changes are minimized.

    b) Specimens are extruded using an extruder system similar to that foreseen in the prospective full-scale application, thus subjecting the tested material to similar shear history and degree of compaction.

    c) The curing of laboratory specimens is adjusted to that planned for the full-scale application, indeed, if planned at all. If specific temperature, humidity, and wind conditions are expected for the full-scale application, the laboratory tests should be performed if possible under similar environmental conditions.

    d) If admixtures are added in the printhead during full-scale applications, the same procedure should be implemented in the lab-scale 3D-printing.

Regarding change of scales, the authors do anticipate that the proposed approach withstand the change in scales, however, with some limitations which need further investigation. So long as the changes are only in dimensions and not in shape of the geometry, the validity of the proposed approach can be seen as convincing. Nevertheless, a correction factor may need to be introduced to take dimensional change into account. Such factors can be identified theoretically/numerically and/or with help of full-scale validation experiments. It goes without saying that in some cases (full-scale applications are large and tall structures) downscaled experiments are the only feasible option to assess the buildability.

Another issue is that downscaling is limited by minimum feasible dimensions of layer cross-section and nozzle dimensions as defined by the maximum aggregate size; this is pointed out in Section 2.2. To extend the range of downscaling, the maximum aggregate size used in mixtures for laboratory experiments may be reduced. This is an approach used sometimes in the practice of construction for various practical reasons such as the availability of appropriate testing equipment, ease of handling *etc*. Certainly, such change in material composition must be well thought through, and its consequences must be closely considered. However, it seems feasible to decrease maximum aggregate size for 3D-printing in laboratory since the effect of maximum aggregate size can be

406 relatively well estimated based on available contemporary knowledge. It is known from [19,20]
407 that the buildability of a printed layer can be expressed in terms of, and proportionally depends on
408 the structural build-up of concrete. MAHAUT *et al.* [32] related the static yield stress of cementitious
409 suspensions with coarse particles $\tau_c(\phi, t)$ to the static yield stress of the suspending cement paste
410 $\tau_c(0, t)$, to the time t passed at rest, and to the coarse particle volume fraction ϕ; see Eq. 19. They
411 suggested that the presence of ϕ, the volume fraction of coarse particles in a cement paste, will
412 magnify its static yield stress as a function of the volume fraction of coarse particles $g(\phi)$.

413 $\tau_c(\phi, t) = \tau_c(0, t)g(\phi)$ Eq. 18

414 $g(\phi) \quad = \sqrt{(1 - \phi)(1 - \phi/\phi_m)^{-2.5\phi_m}}$ Eq. 19

415 where ϕ_m is the maximum volume fraction.

416 In addition Mahaut *et al.* [32] postulated that "the structuration rate A_{thix} has the same dependence
417 on the coarse particle volume fraction as the yield stress". Similar models for relating properties
418 of a suspension to suspending paste are presented and discussed in [33–35]. These findings imply
419 that the parameters identified through a proposed approach on a concrete with finer aggregates
420 could be applied to concrete with coarse aggregates using a factor similar to that of Eq. 19.
421 However, this hypothesis is yet to be verified.

3. Applying proposed buildability criteria to CONPrint3D

423 Generalized buildability criteria proposed above in Section 2 are applied here to an on-site concrete
424 3D-printing technology, CONPrint3D. On completion of this section, the specifications of
425 buildability tests on cementitious materials applicable for CONPrint3D are clearly derived. As
426 elaborated in Section 2, these necessary specifications are: height of the experimental wall to be
427 printed, number of layers in this wall, and the time interval (TI) between the layers. While the target
428 full-scale implementation of CONPrint3D technology will be primarily with coarse-grained
429 aggregates, of maximum aggregate size 8 mm to 16 mm, the use of fine-grained concrete should
430 not be excluded, certainly not at this stage, since it has many advantages with respect to processing
431 and the maturity of the extrusion machine technology required, "lightness" of the printhead, *etc*.
432 Thus, as a first step the validation presented below will consider an application case of
433 CONPrint3D where fine-grained concrete is used. The reason behind this is that the validation can
434 be performed directly without need for additional assumptions or specific correcting factors. In a
435 follow up study, the proposed buildability criteria will be applied to 8 mm aggregate, printable
436 concrete, and if necessary adjustment of the approach will be made. Note that the higher material
437 costs of fine-grained concrete are taken into account in Section 3.2.

3.1 Height of the wall specimen and number of layers to be tested

439 Of the primary target applications for the CONPrint3D approach, one- to multi-story residential
440 buildings [5,8] make up an important segment; see Figure 5. Table 2 presents the dimensions of the
441 corresponding outer and inner walls for each story. Also presented are the nozzle dimensions
442 employed for the lab-scale 3D-printing testing device (3DPTD), which was designed in 2015 at the
443 TU Dresden and has been used since then for material development. Furthermore, Table 2 presents
444 various extra cases, namely Inner, Outer2 and Outer3. These cases provide additional information

445 on how $H_{min,exp}$ and n_{layers} vary depending on wall and nozzle dimensions. $H_{min,exp}$ and n_{layers}
446 are calculated using Eq. 9 and Eq. 11. These calculations highlight the consideration of layer
447 geometry in the proposed buildability criteria. If the laboratory nozzle breadth is increased and
448 laboratory nozzle height remains unchanged, then the height $H_{min,\text{exp}}$ to be tested in the laboratory
449 also increases. If the thickness of the target wall decreases, as in the case of inner walls, then
450 $H_{min,\text{exp}}$ increases. Similarly, if the height of the printed layer, i.e. nozzle in the lab, increases
451 where its breadth remains unchanged, then the number of layers to be printed in the laboratory tests
452 will decrease. These variations of buildability test specifications are crucial, considering that the
453 nozzle dimensions in the laboratory printers may vary significantly even though the final targeted
454 element (application) dimensions and the geometry of the real-application printhead do not change.
455
456 *Table 1:   Dimensions of the target application and corresponding calculated parameters for laboratory*
457 *buildability testing.*

	Parameter	Unit	Outer	Inner	Outer2	Outer3
Application	Wall height	m	2.500	2.500	3.000	2.500
	Wall breadth	m	0.240	0.175	0.240	0.240
	Aspect ratio		10.417	14.286	12.500	10.417
Lab	Layer breadth	m	0.030	0.030	0.030	0.060
	Layer thickness	m	0.020	0.020	0.020	0.020
	Height to be tested	m	0.313	0.429	0.375	0.625
	No of layers	#	16	21	19	31

458 The material explicitly considered in this article is a high-strength, fine-grained concrete M, its
459 compressive strength at an age of 28 days exceeding 80 MPa, developed for the outer load-bearing
460 walls of the target residential buildings. Thus, for the laboratory buildability tests, case 'Outer'
461 presented in Table 2 will be considered. Table 2 shows that to ascertain the buildability of the
462 mixture *M*, 16 layers have to printed in the laboratory, complying with maximum time-interval and
463 prescribed tolerances, for example, according to the German standard DIN 18202:2013-04 [26]).
464 The handling of the cases other than Outer should follow the same routine.

465

Figure 5: *Sketch of a representative target residential building.*

3.2 Time interval (TI)

The calculations presented below are valid for walls of one floor of a multi-story house erected using CONPrint3D; for purposes of comparison an estimation for walls made of conventional masonry are provided too. The process parameters of masonry construction are given in Table 2; here the use of sand-lime bricks is assumed. These are used to calculate the construction costs for the masonry work and to derive $V_{DC,min}$.

Table 2:   Dimensions of the target application and process parameters of example masonry constructions

	Parameter	Unit	Outer	Inner	Outer2	Outer3
Applica-tion	Wall height	m	2.500	2.500	3.000	2.500
	Wall length	m	43.040	19.860	43.040	43.040
	Wall breadth	m	0.240	0.175	0.240	0.240
Masonry	Inversed rate of construction	h/m^2	0.6	0.6	0.6	0.6
	Machine costs	€/h	14	14	14	14
	Labor costs per person	€/h	35	35	35	35
	No. of workers	person	3	3	3	3
	Material costs	€/m^3	164.05	164.05	164.05	164.05

The outer wall length of 43.04 m and the inner wall length of 19.86 m as presented in Table 2 are calculated from the floor layout of the target application, presented in Figure 6. To calculate the printhead travel length for each layer to be deposited, it is essential to address "printing scenarios" or the aspect of "tool-path optimization". For the sake of simplicity, in the example presented here we assume that one complete layer along the outer walls is printed first. Subsequently, further layers of the outer walls are added upon one another. After the completion of the outer walls, the inner walls are produced and frictionally connected to the outer walls by stainless steel anchors, which are inserted into each layer. In contrast to this simple scenario, the path of the printhead can be defined in numerous ways, as shown in Figure 7, while various algorithms can be utilized for determining the optimum printing scenario. In such cases, the wall length in Table 3, must be adjusted according to the printing path finally chosen.

485 It is noteworthy that the choice of a suitable starting point and the minimization of *idle-traverses*
486 (travel times without concrete discharge, shown with the dashed line in Figure 7) are of great
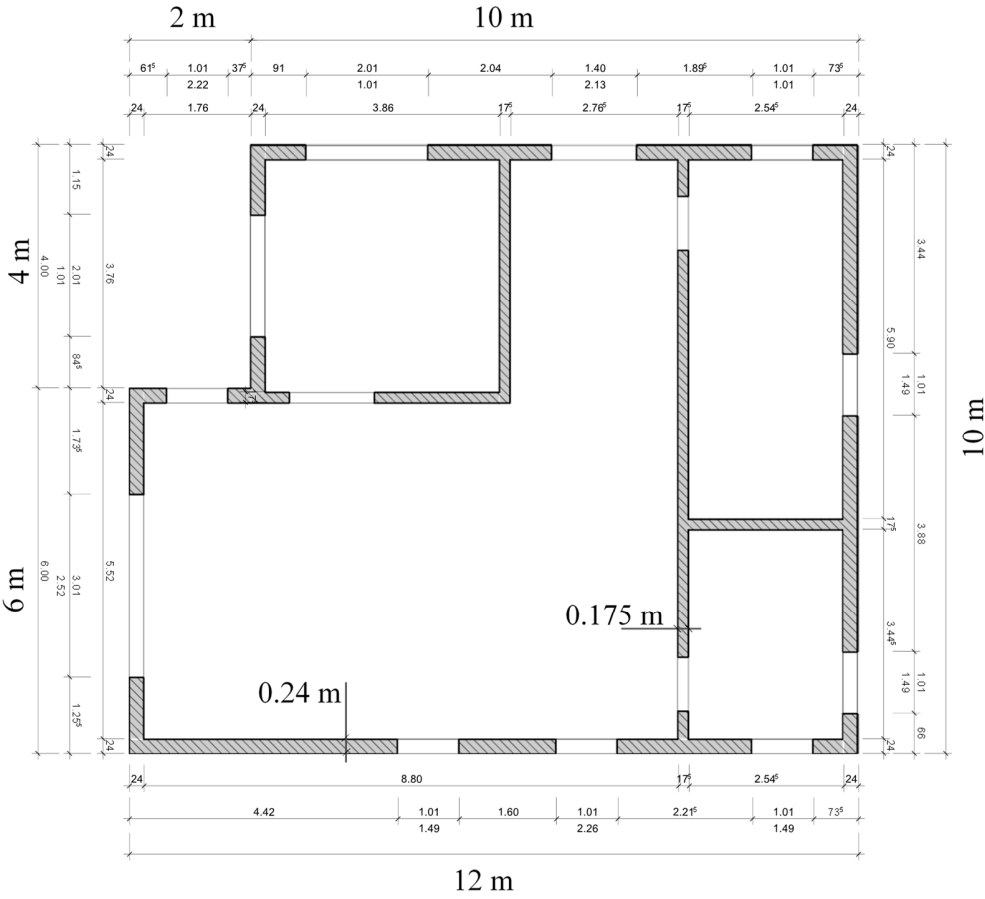487 importance in any printing strategy.

Figure 6: Layout and dimensions of a storey of the target house.

490 The optimal printing path depends on numerous boundary conditions. An essential optimization
491 criterion is the path length. While the shortest printing path should be generally preferred, it cannot
492 always be used due to other constraints, such as the motion and clearance profiles of the printhead
493 or on-site construction process conditions. Zhang *et al*. [36] adapted the so-called "traveling
494 salesman problem (TSP)" to determine the optimal tool path for constructing with Contour Crafting
495 technology. They derived the shortest paths by adding multiple vertices in the corners and wall
496 connections, and then by transforming the optimization problem from the node-oriented to the
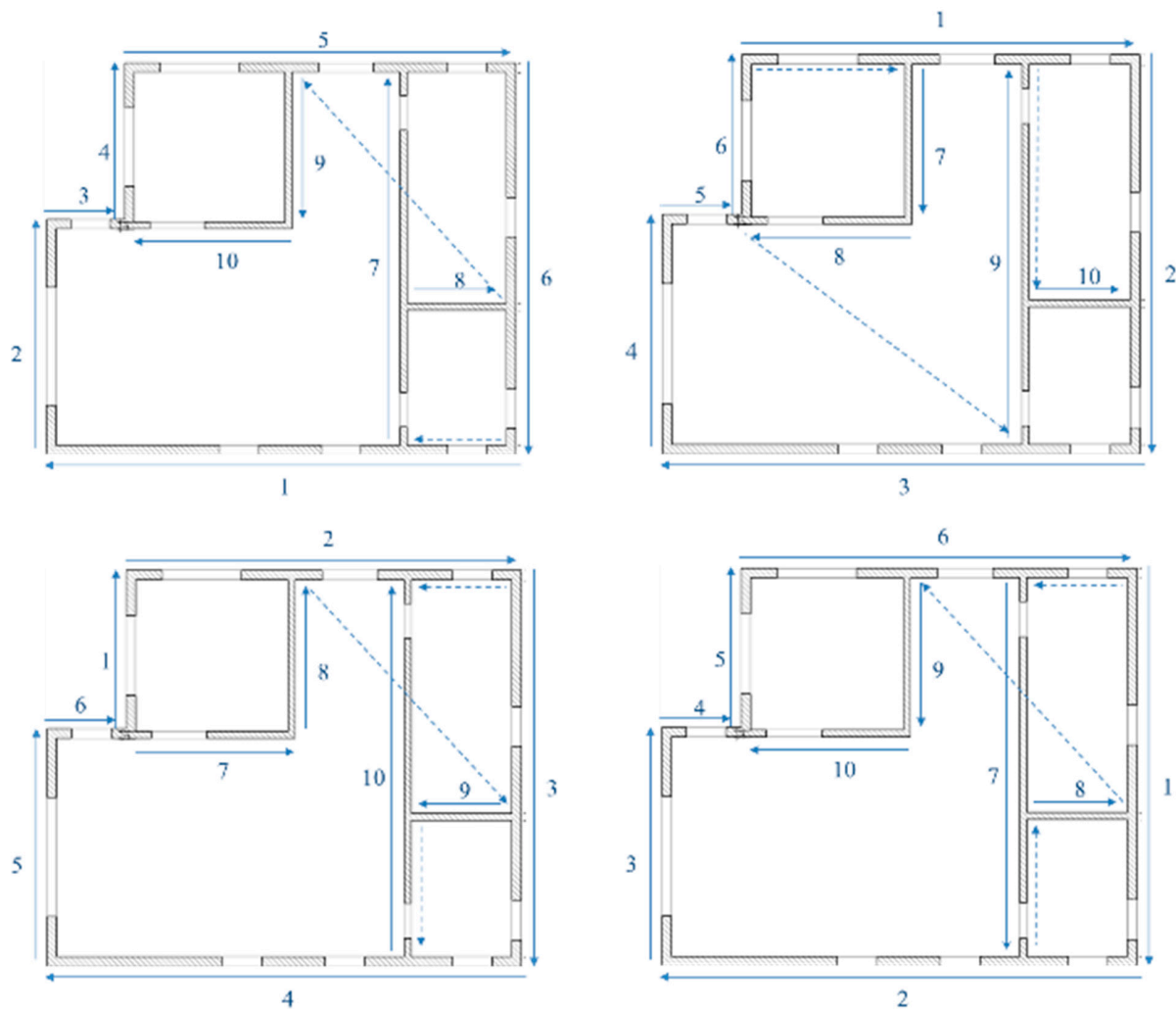497 edge-oriented view.

498

499
500
Figure 7: Various scenarios for printing the walls of a house considered under consideration.

501   The rate at which masonry construction takes place is generally expressed in terms of the time
502   needed to complete a square meter of a wall, usually an hour. Since this rate is inverse to the rate
503   generally considered in concrete construction rates, i.e., unit area per unit time, more specifically
504   square meters per hour, it is termed here *inversed rate of construction* with a notation *RI;* see
505   Section 2. The RI values used in the articles at hand are according to
506   *Baukosteninformationszentrum Deutscher Architektenkammern* (BKI) for the masonry wall type
507   KS-L-R 8 DF 240 mm [37]. The rate of construction is given per person, thus, when deriving V_{DC}
508   using Eq. 17, one must multiply *RI* with actual number of workers working on the masonry
509   application, which is in this case three, leading to an effective *RI* of 0.2 h/m^2.

510   Machine costs presented in Table 4 for a small crane (Kleinkran C.2.00.0007I) are in accordance
511   with BGL 2015 [38]. These costs include repair, depreciation and interest costs. The material costs
512   are also calculated for the masonry wall type Format KS-L-R 8 DF 240 mm and include delivery
513   and mortar costs [37]. Process parameters of the CONPrint3D are presented in Table 4, which are
514   used to calculate the construction costs and derive $V_{DC,min}$.

515 *Table 3:   Process parameters for the application of CONPrint3D*

	Parameter	Unit	Outer	Inner	Outer2	Outer3
CONPrint3D	Layer thickness	m	0.160	0.117	0.160	0.160
	Layer breadth	m	0.240	0.175	0.240	0.240
	Machine costs	€/h	140	140	140	140
	Labor costs (2 persons)	€/h	70	70	70	70
	Material costs	€/m³	130	130	130	130

516 Since CONPrint3D is an FWP process, the breadth of the printed layer is equal to the breadth of
517 the target wall. For the case "Outer" considered here, the breadth of a printed layer is 0.24 m. The
518 thickness of the layer is a process parameter which affects the total number of layers to be printed,
519 total printing time, and hence construction costs. The maximum feasible layer thickness depends
520 on the material properties. For the case presented here, layer thickness was assumed to be two-
521 thirds of the layer breadth in accordance with the geometrical proportions of the nozzle of the lab
522 printer. Numerous scaled-down wall-elements, including those in Figure 4, had been already
523 printed using the aforementioned nozzle-aspect ratio. Machine costs for CONPritn3D as given in
524 Table 4 are, at the current stage, higher than that of masonry construction. They include costs for a
525 modified concrete boom pump, costs for transporting concrete from mixing plant to construction
526 site and costs for adjusting and calibrating the pump on the site. In general, for DC technologies
527 lower manpower costs are envisioned in comparison to conventional construction. In the case of
528 CONPrint3D two workers would be necessary from today's perspective: one for machine
529 monitoring and one for auxiliary works. Based on BKI 2017 values, the average wage of one
530 person is calculated at 35 € per hour [37].

531 The material costs for CONPrint3D, 130.00 €/m³, are calculated conservatively for high-strength,
532 fine-grained concrete M used in experiments. They include material costs for admixtures and
533 additives (micro-silica suspension, fly ash and superplasticizer). In sum, the material costs are
534 approximately 70 % higher in comparison to the material costs for ordinary concrete of the strength
535 class C25/30 in conventional construction. The mixture M, containing expensive additives and
536 admixtures, was chosen deliberately for the calculations to ensure process-safe implementation of
537 the onsite digital construction of load-bearing elements since printable concrete is, in general, likely
538 to contain fine mineral additives and chemical admixtures to achieve the required rheological,
539 mechanical and/or durability characteristics. While for the target residential building application,
540 the required concrete class according to DIN EN 206-1 is C25/30. The fine-grained concrete
541 considered here has a compressive strength of 100 MPa at an age of 28 days. Thus, a considerable
542 reduction in material costs is feasible in the course of the optimization process. In addition to
543 material, machine and labor costs, 10 % additional costs are added to the total costs of CONPritn3D
544 as detailed in Section 2.

545 The minimum average printhead velocity $V_{dc,min}$ for CONPritn3D application, to be equally
546 economically viable with masonry construction, is calculated using Eq. 17 and data from Tables 2

547   through 4. After knowing $V_{dc,min}$ the maximum (again economically viable) *TI* between layers can
548   be calculated as $TI = L_t / V_{dc,min}$. Table 5 presents both $V_{dc,min}$ and maximum *TI* calculated for various
549   cases of CONPrint3D application. For the Outer case, the time interval between extruding
550   subsequent layers should not exceed 51.61 minutes. In addition to the maximum *TI* it is also
551   possible to define the minimum *TI* based on the maximum printing speed of the printer to be used.
552   Since the current laboratory printer for CONPrint3D has $V_{dc,max}$ = 540.00 m/h, the minimum feasible
553   time interval can be calculated as $TI = L_t / V_{dc,max}$. The minimum *TI* for the Outer case is 4.78
554   minutes; see Table 5. It goes without saying that if printing of the entire construction were to occur
555   at a rate close to $V_{dc,max}$ then the costs and construction time in case of CONPritn3D will be
556   considerably reduced in comparison to those of conventional construction.

557   *Table 4:   Process parameters of an example CONPrint3D application.*

Parameter	Unit	Outer	Inner	Outer2	Outer3
$V_{dc,min}$	m/h	50.04	72.04	50.04	100.08
Maximum *TI*	min	51.61	16.54	51.61	51.61
$V_{dc,max}$	m/h	540.00	540.00	540.00	540.00
Minimum *TI*	min	4.78	2.21	4.78	4.78

558   **3.3 Experimental validation**

559   For production of the wall specimens, a custom-developed 3D-concrete-printing test device
560   (3DPTD) was used; see Figure 8. The 3DPTD is equipped with a progressive cavity pump to
561   extrude concrete. The speed at which a layer is printed and the time interval between the deposition
562   of two consequent layers can be pre-programmed. Details of the mechanical and electrical setup of
563   3DPTD are to be published elsewhere. The buildability of a fine-grained concrete *M* was validated
564   using the criteria proposed above. The composition of *M* can be found in [39]. The target
565   application considered is a residential house; see Section 3.1 and Figure 5. Specifically for the case
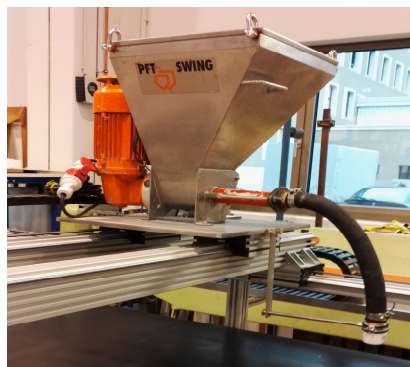566   Outer see Tables 3 to 5.

567

568   ***Figure 8:** Printhead of 3DPTD consisting of concrete hopper, progressive-cavity extruder and nozzle.*

569   The design of the buildability experiment is to produce n_{layers} number of layers with *TI* minutes
570   of time interval between layers. If the printed wall retains its geometry and dimensions then the
571   tested material is applicable for the target application. As determined in Sections 3.1 and 3.2, a
572   total of 16 layers with maximum time intervals of 61.24 minutes must be printed. The time-interval

573   mentioned here is the upper limit. *TI* longer than 61.24 minutes adversely affects economic viability
574   if all other parameters are assumed constant. At a concrete age of 20 minutes from water addition
575   printing experiments were started by printing layers at a constant velocity of 150 mm/s and time
576   intervals of 3 minutes. Figure 9 shows the wall immediately after completion of the printing. Since
577   16 layers could be printed with a *TI* much shorter than the economically required *TI,* the mixture
578   *M* could be designated "buildable" for the considered application case.

579   ***Figure 9:*** *16-layer wall specimen printed using fine-grained concrete M with time intervals of 3 minutes between*
580   *layers.*

4. Buildability requirements for filament printing and full-width printing

582   Buildability requirements for a material depend not only upon the target structure but also on the
583   printing approach applied. The 'height' component of the buildability criteria remains essentially
584   the same for both the full-width printing (FWP) and filament printing (FP) approaches. In contrast,
585   the 'effective length' of each layer to be printed, i.e. total travel distance, often greater than the
586   length of the actual wall, varies significantly between FWP and FP, which directly affects *TI* as
587   well. If a single-nozzle opening is used, as in [2,4,5,10,40], in the case of FP, the printhead travels
588   approximately twice the distance in comparison to FWP to complete the deposition of the outer
589   filaments; see Figure 10. Furthermore, additional time is needed to place the inner wave-like
590   filament. Since in the case of full-width printing the entire layer cross-section is printed in one run,
591   printhead velocity $V_{printhead,FWP}$, the velocity calculated using **distance** travelled by the printhead,
592   is equal to the "effective" horizontal velocity of printing $V_{effective,FWP}$, velocity being calculated
593   using **displacement** along the wall length. For FP, in contrast, even if printhead velocity $V_{printhead,FP}$
594   is kept the same as $V_{printhead,FWP}$, the "effective" horizontal velocity of construction $V_{effective,FP}$ will
595   be lower than $V_{effective,FWP}$. Consequently, to achieve an equal construction rate in the case of FP,
596   printhead velocity $V_{printhead,FP}$ has to be much higher than in the case of FWP. A simplistic
597   approximation for FP can be:

598    $V_{printhead,FP} = V_{effective,FP}\ (2+k)$ with $k = f(\lambda, \hat{u})$ *Eq. 20*

599   where λ is the wavelength and $\hat{u}$ is the amplitude of the wave depicting the inner filament of the
600   wall produced by means of FP; see Figure 10c.

601   Since the $V_{effective}$ of FP is much lower than that of FWP the TI between layers in case of FP is also
602   longer. Although it may appear advantageous in terms of "available" resting time for structural
603   build-up, a longer TI means a reduction in the economic viability and a higher risk of formation of
604   "cold joints", weak interface strengths, between layers. Savings in material through FP in
605   comparison to FWP are less significant: as Tables 3 and 4 show, material costs are not the major
606   contributor for the total construction costs.

607   From a rheological perspective, Eq. 20 implies the following two cases summarized in Table 5,
608   where FP is compared to FWP for the same target application.

609   *Table 5:   Requirements in case of FP depending on the comparative constant.*

	Comparative cases of FP and FWP	FP requires
1	Constant economic viability	• Higher $V_{printhead,FP}$ • Higher rates of material pumping and extruding, thus higher pumpability and extrudability. • Lower plastic viscosity.
2	Constant printhead speed $V_{printhead}$	• Lower buildability (TI will be higher) • higher open-time/working-window of the construction material • Longer construction times

610   It is of interest mathematically to describe the above-mentioned intricacies of buildability
611   requirements for FP and FWP in order to facilitate:

612   • Choice between FP and FWP, if the choice of material is restricted;
613   • Extension of the model presented in Section 2 to FP cases by providing a mathematical
614   description of TI in terms of wall geometry, for instance, the minimum TI in the case of FP
615   be calculated using Eq. 30-32;
616   • Development of process-agnostic, printable concretes, i.e. concretes applicable for both FP
617   and FWP processes.

618   The following is the derivation for the needed $V_{printhead,FP}$ in relation to $V_{printhead,FWP}$, provided only
619   one nozzle is used and constant economic viability or constant construction rate is to be achieved
620   (Case 1 in Table 5).

621

622   Assuming

623   • length of the wall to be produced: *L*,

624   • distances that the printhead travels in case of FWP (Figure 10a): *L1,*

625   • distances that printhead travels in case of FP (Figure 10b, -c): *L2* for outer and *L3* for inner

626   profile,

627   we obtain:

628   time for printhead travel in FWP: $t_{FWP} = L1/V_{printhead,FWP} = L1/V_{effective,FWP}$ and

629   time for printhead travel in FP: $t_{FP} = (L2+L2+L3)/V_{printhead,FP}$.

630   Assuming equal economic viability in FP and FWP as in Case 1 (Table 5), both the times should

631   be equal, thus:

632    $$\frac{L1}{V_{effective,FWP}} = \frac{L2+L2+L3}{V_{printhead,FP}}$$ *Eq. 21*

633    $$V_{printhead,FP} = \left(\frac{L2+L2+L3}{L1}\right) V_{effective,FWP}$$ *Eq. 22*

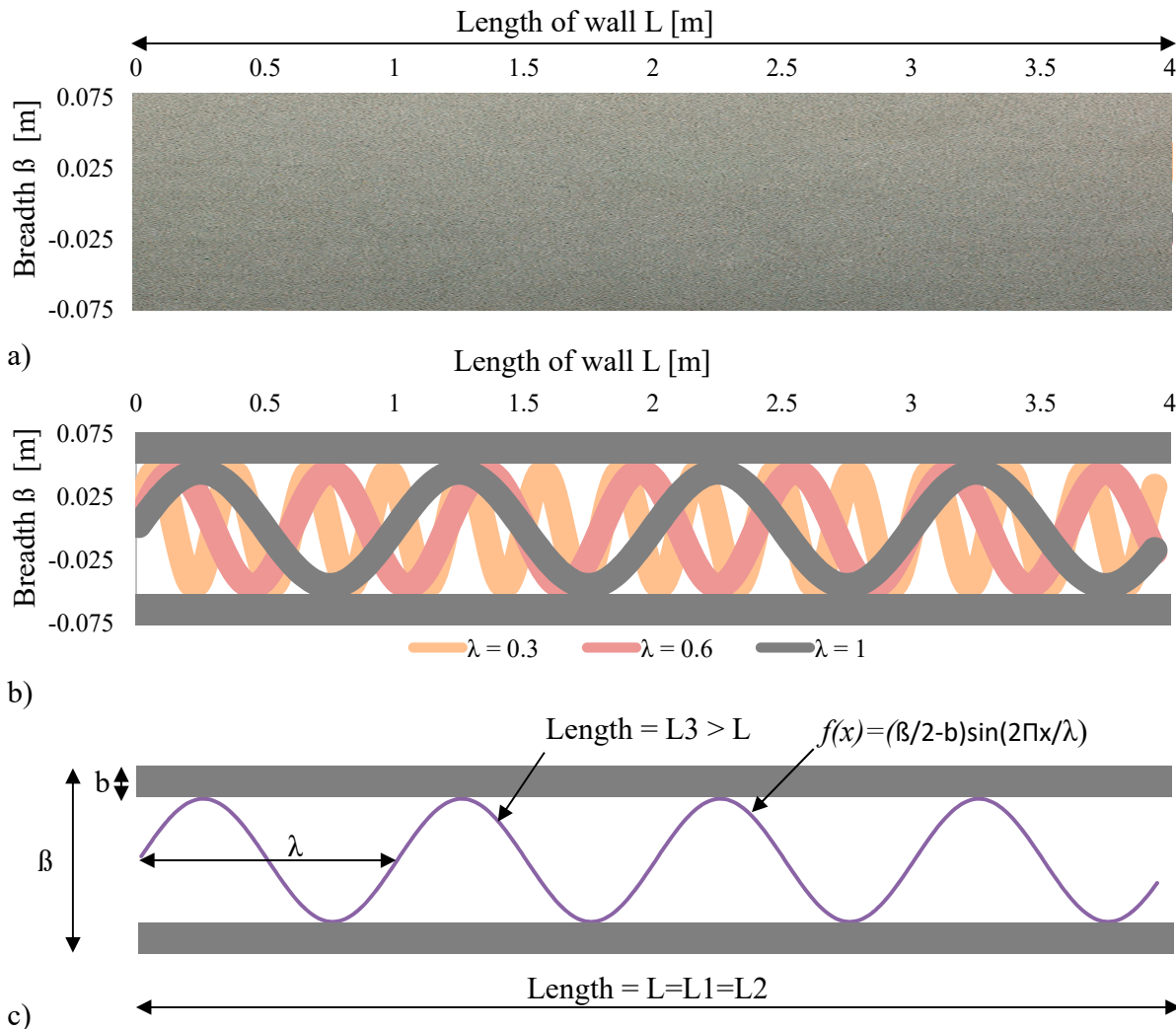
634   a)

635   b)

636   c)

637   **Figure 10:** *Schematic views of the top sectional views of two walls of identical length and width, produced through*

638   *a) full-width-printing FWP) and b) filament-printing FP. The FP figure also illustrates two additioanl alternatives*

639   *for inner filament defined by wavelengths λ. c) A scheme showing wavelength and semi-amplitude of sinusoid*
640   *dipcting inner filament in FP.*

641   Since the length of the wall $L = L1 = L2 \neq L3$ *Eq. 23*

642    $V_{printhead,FP} = \left(2 + \frac{L3}{L}\right) V_{effective,FWP}$ *Eq. 24*

643   Expressing the inner filament in FP as a sinusoid $y = i \sin j\, x$ from 0 to L

644   Length (distance between 0 and L) of the inner filament is

645    $L3 = \int_0^L \sqrt{1 + ((i*j)\cos^2 j\, x}\; dx$ *Eq. 25*

646   With i = semi-amplitude of the inner filament = $\hat{U} = ß/2-b$

647   and $j = 2\Pi/\lambda$

648   where $ß$ and b are the breadth of the produced wall and filament, respectively, and λ is the
649   wavelength of the inner filament; see Figure 10c.

650   Length of the inner filament expressed in sinusoid attributes can be calculated according to Eq.
651   26:

652    $L3 = \int_0^L \sqrt{1 + ((\frac{ß}{2} - b)*\frac{2\pi}{\lambda})\cos^2 \frac{2\pi x}{\lambda}}\; dx$ *Eq. 26*

653   From Eq. 17 and Eq. 19 we obtain:

654    $V_{printhead,FP} = \left(2 + \frac{\int_0^L \sqrt{1+((\frac{ß}{2}-b)*\frac{2\pi}{\lambda})\cos^2\frac{2\pi x}{\lambda}}\; dx}{L}\right) V_{effective,FWP}$ *Eq. 27*

655   Equation 27 enables determination of printhead velocity to be followed while applying FP to retain
656   economic viability equal to that of FWP processes.

657   Still further, if equal economic viability is not the primary concern and constant printhead speed is
658   followed for both FP and FWP, i.e. Case 2 in Table 5, then a higher minimum *TI* is valid for FP.
659   The following relationship between $TI_{min,FP}$ and TI_{minFWP} can be obtained:

660    $TI_{min,FP} = \left(\frac{Travel\ length\ in\ case\ of\ FP}{Travel\ length\ in\ case\ of\ FWP}\right) TI_{min,FWP}$ *Eq. 28*

661    $TI_{min,FP} = \left(2 + \frac{\int_0^L \sqrt{1+((\frac{ß}{2}-b)*\frac{2\pi}{\lambda})\cos^2\frac{2\pi x}{\lambda}}\; dx}{L}\right) TI_{min,FWP}$ *Eq. 29*

662   In addition, with no comparison to FWP, the minimum *TI* in case of FP can be calculated for a
663   printhead velocity of $V_{printhaed}$:

664    $TI_{min,FP} = \frac{2L + \int_0^L \sqrt{1+((\frac{ß}{2}-b)*\frac{2\pi}{\lambda})\cos^2\frac{2\pi x}{\lambda}}\; dx}{V_{printhead}}$ *Eq. 30*

665   Eq. 30 is a generalized formula to determine the minimum time intervals between layers, which
666   formula must be followed during laboratory buildability tests if an element of target length L is
667   produced through FP.

668   It must be noted that Eq. 30 is valid only if one nozzle is used to print the filaments; see Figure
669   11a. If more than one nozzle is used for printing, then the following scenarios can be followed:

670 a) Two passes are needed for one horizontal layer of the target wall. In the first pass, two
671   nozzles extrude the outer 'shells' and in the second pass, one nozzle extrudes the inner
672   'wave'; see Figure 11b. An example of this scenario is demonstrated by Contour Crafting
673   [41].
674 b) One pass is needed for one horizontal layer of target wall. Two nozzles extrude the outer
675   'shells' and in parallel, a third nozzle prints the inner 'wave'. To the best of authors'
676   knowledge, this scenario has not yet been demonstrated.

677 Moreover, in both scenarios one additional pass of the printhead or other devise will be needed if
678 spaces between 'shells' and 'wave' need to be filled, e.g. with insulating materials or (self-
679 compacting) concrete; see Figure 11c.

680 For the scenarios 'a' and 'b' mentioned above, Eq. 30 can be transformed to Eq. 31 and Eq. 32,
681 respectively:

682
$$V_{printhead,FP} = \left(1 + \frac{\int_0^L \sqrt{1+\left(\left(\frac{\text{ß}}{2}-b\right)*\frac{2\pi}{\lambda}\right)\cos^2\frac{2\pi x}{\lambda}}\,dx}{L}\right) V_{effective,FWP} \qquad \text{Eq. 31}$$

683
$$V_{printhead,FP} = \left(\frac{\int_0^L \sqrt{1+\left(\left(\frac{\text{ß}}{2}-b\right)*\frac{2\pi}{\lambda}\right)\cos^2\frac{2\pi x}{\lambda}}\,dx}{L}\right) V_{effective,FWP} \qquad \text{Eq. 32}$$

684 Similarly, Eq. 29 and Eq. 30 can be reformulated according to the number of nozzles used. As can
685 be seen in Eq. 32, even if three nozzles are used and moved at the same speed as in case of FWP,
686 the effective printing velocity in case of FP will be lower in comparison to FWP due to the longer
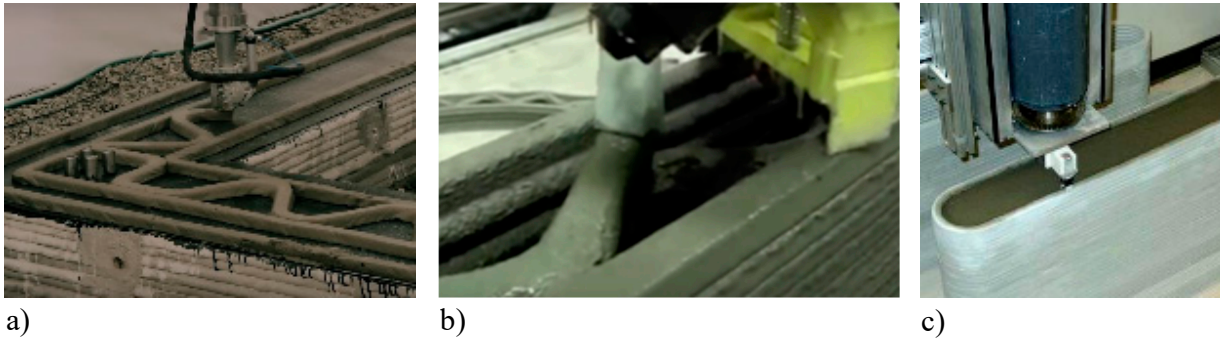687 absolute traveling length.

a)   b)   c)

688
689 ***Figure 11:*** *Various scenarios for printing "one set of horizontal layers" in case of FP printing process: a) single*
690 *nozzle – three passes are needed* [42]*, b) three nozzles – two passes are needed* [41] *and c) representation of single*
691 *nozzle with "post-filling" of the empty space between layers* [43]*.*

692 Based on the deduced relationships, it can be concluded that when testing the buildability of a
693 material for FP processes, generally higher velocities of the printhead are to be followed during
694 laboratory tests in comparison to corresponding tests for FWP.

695

5. Conclusions and outlook

Buildability, i.e. the ability of extruded material to retain its shape and size under sustained loads, has been critically examined in the context of digital construction (DC). Practice-oriented buildabiltiy criteria directly linked to their target applications have been proposed herewith. This approach takes machine, labor, and material costs into consideration and so is applicable for quantifying the economic viability of DC processes. The height of the wall to be printed and the time interval between layers were identified as the primary specifications for laboratory buildability tests needed to validate the choice of material and process parameters. The height of the experimental wall was calculated using the aspect ratio of the target construction element. Maximum time interval was determined considering the minimum printing velocity needed for DC to be economically viable in comparison with conventional construction.

In case of CONPrint3D application for a residential building, a lab-scale wall of 16 layers with a maximum time interval of approximately 52 minutes was determined as the buildability test criterion. The buildability of a fine-grained, printable concrete was validated for this application scenario. It was also proven that the buildability criterion for a given material not only depends upon the target structure, but also on the applied printing process/approach. The comparative analyses of full-width printing (FWP) and filament printing (FP) revealed that, assuming the same rate of construction, the buildability of a material for FP processes should be tested at higher velocities of the printhead in corresponding laboratory experiments than in the case of FWP. In addition, a constitutive relationship was derived to calculate the printhead velocity needed in the case of FP related to the velocity in FWP, to achieve an equal construction rate.

Some issues raised in the article at hand are subject of ongoing research. The main activities, actual or planned, can be summarized as follows:

- Validation of the approach with full-scale printing tests, with printable concretes containing aggregates with a maximum size of 8 mm.
- Simplification of the proposed approach: A representative piece of wall should be printed in the lab using the same filament geometry as in the real application, however, consisting of a few layers only, while after completion of the printing vertical, stepwise increasing load is applied on this piece. The increase in load should follow the defined time intervals to mimic the deposition of further layers, while measuring deformations. This approach is in principle similar to that proposed by Perrot [20], but different in terms of specimen production (3D-priting instead of casting), geometry and underlying buildability criteria (not based on rheological tests). Most importantly, the question of what a representative piece of the wall to be tested in the lab is and what the time intervals to be tested are to call a material printable can be quantified directly with the approach suggested in the article at hand.
- Direct buildability tests at various ambient conditions (temperature, humidity, wind velocity).

Acknowledgements

736   **References**

[1]   B. Khoshnevis, Automated construction by contour crafting—related robotics and
        information technologies, Autom. Constr. 13 (2004) 5–19.
        doi:10.1016/j.autcon.2003.08.012.

[2]   R.A. Buswell, R.C. Soar, A.G.F. Gibb, A. Thorpe, Freeform Construction: Mega-scale
        Rapid Manufacturing for construction, Autom. Constr. 16 (2007) 224–231.
        doi:10.1016/j.autcon.2006.05.002.

[3]   E. Dini, Monolite-UK-Ltd, D-Shape, (2015). https://d-shape.com/ (accessed August 23,
        2015).

[4]   TotalKustom, 3D-Printed Hotel, (2015). http://www.totalkustom.com/3d-printed-hotel-
        suite.html (accessed April 27, 2016).

[5]   V.N. Nerella, M. Krause, M. Näther, V. Mechtcherine, 3D printing technology for on-site
        construction, Concr. Plant Int. 4 (2016) 36–41.

[6]   C. Gosselin, R. Duballet, P. Roux, N. Gaudillière, J. Dirrenberger, P. Morel, Large-scale
        3D printing of ultra-high performance concrete – a new processing route for architects and
        builders, Mater. Des. 100 (2016) 102–109. doi:10.1016/j.matdes.2016.03.097.

[7]   E. Lloret, A.R. Shahab, M. Linus, R.J. Flatt, F. Gramazio, M. Kohler, S. Langenberg,
        Complex concrete structures - Merging existing casting techniques with digital fabrication,
        Comput. Des. 60 (2015) 40–49. doi:10.1016/j.cad.2014.02.011.

[8]   R. Schach, M. Krause, M. Näther, V.N. Nerella, CONPrint3D: 3D-Concrete-Printing as an
        Alternative for Masonry, Bauingenieur. 9 (2017) 355–363.
        http://www.bauingenieur.de/bauing/article.php?data[article_id]=88138 (accessed October
        18, 2017).

[9]   D. Weger, D. Lowke, C. Gehlen, 3D printing of concrete structures using the selective
        binding method – Effect of concrete technology on contour precision and compressive
        strength, in: 11th Fib Int. PhD Symp. Civ. Eng. FIB 2016, A.A. Balkema Publishers,
        University of Tokyo, Tokyo, 2016: pp. 403–410.

[10]   Mike Murphy, Apis Cor can 3D-print an entire house in just one day, Quartz. (2017) 1.
        https://qz.com/924909/apis-cor-can-3d-print-and-entire-house-in-just-one-day/ (accessed
        March 8, 2017).

[11]   M. Hansmeyer, B. Dillenburger, Digital Grotesque I, (2014). http://www.michael-
        hansmeyer.com/projects/digital_grotesque.html?screenSize=1&color=1#21.

[12]   WinSun, 3D Printing Construction - Project web page, (2015).
        http://www.yhbm.com/index.php?m=content&c=index&a=lists&catid=67 (accessed
        August 23, 2015).

[13]   TU Eindhoven, TU Eindhoven starts using kingsize 3D concrete printer, (2015) 3–4.
        https://www.tue.nl/en/university/news-and-press/news/22-10-2015-tu-eindhoven-starts-
        using-kingsize-3d-concrete-printer/.

[14]   S. Lim, R. Buswell, T. Le, R. Wackrow, S. Austin, A. Gibb, T. Thorpe, Development of a
        Viable Concrete Printing Process, in: Proc. 28th Int. Symp. Autom. Robot. Constr., Seoul,
        South Korea, 2011: pp. 665–670. doi:10.22260/ISARC2011/0124.

[15]   T.T. Le, S. A. Austin, S. Lim, R. A. Buswell, A. G.F. Gibb, T. Thorpe, Mix design and fresh properties for high-performance printing concrete, Mater. Struct. 45 (2012) 1221–1232.

[16]   V. Mechtcherine, V.N. Nerella, K. Kasten, Testing pumpability of concrete using Sliding Pipe Rheometer, Constr. Build. Mater. 53 (2014) 312–323. doi:10.1016/j.conbuildmat.2013.11.037.

[17]   M. Choi, N. Roussel, Y. Kim, J. Kim, Lubrication layer properties during concrete pumping, Cem. Concr. Res. 45 (2013) 69–78. doi:10.1016/j.cemconres.2012.11.001.

[18]   D. Feys, K.H. Khayat, R. Khatib, How do concrete rheology, tribology, flow rate and pipe radius influence pumping pressure?, Cem. Concr. Compos. 66 (2016) 38–46. doi:10.1016/j.cemconcomp.2015.11.002.

[19]   T. Wangler, E. Lloret, L. Reiter, N. Hack, F. Gramazio, M. Kohler, M. Bernhard, B. Dillenburger, J. Buchli, N. Roussel, R. Flatt, Digital Concrete: Opportunities and Challenges, RILEM Tech. Lett. 1 (2016) 67–75. doi:10.21809/rilemtechlett.2016.16.

[20]   A. Perrot, D. Rangeard, A. Pierre, Structural built-up of cement-based materials used for 3D-printing extrusion techniques, Mater. Struct. 49 (2016) 1213–1220. doi:10.1617/s11527-015-0571-0.

[21]   R.J.M. Wolfs, F.P. Bos, T.A.M. Salet, Early age mechanical behaviour of 3D printed concrete: Numerical modelling and experimental testing, Cem. Concr. Res. 106 (2018) 103–116. doi:10.1016/j.cemconres.2018.02.001.

[22]   A. Perrot, A. Pierre, S. Vitaloni, V. Picandet, Prediction of lateral form pressure exerted by concrete at low casting rates, Mater. Struct. 48 (2015) 2315–2322. doi:10.1617/s11527-014-0313-8.

[23]   N. Roussel, A thixotropy model for fresh fluid concretes: theory validation and applications, Cem Concr Res. 36 (2006). doi:10.1016/j.cemconres.2006.05.025.

[24]   N. Roussel, C. Lanos, Plastic fluid flow parameters identification using a simple squeezing test, Appl. Rheol. 13 (2003) 132–139.

[25]   J. Engmann, C. Servais, A.S. Burbidge, Squeeze flow theory and applications to rheometry: A review, J. Nonnewton. Fluid Mech. 132 (2005) 1–27. doi:10.1016/j.jnnfm.2005.08.007.

[26]   Deutsches-Institut-für-Normung-e.-V., DIN 18202:2013-04 - Tolerances in building construction - Buildings, Beuth Verlag, Germany, 2013.

[27]   D. Feys, G. De Schutter, K.H. Khayat, R. Verhoeven, Changes in rheology of self-consolidating concrete induced by pumping, Mater. Struct. 49 (2016) 4657–4677. doi:10.1617/s11527-016-0815-7.

[28]   American Concrete Pumping Association, CONCRETE 101 - A guide to understanding the qualities of concrete and how they affect pumping, 2008 .

[29]   National Ready Mixed Concrete Association, CIP 21 - Loss of Air Content in Pumped Concrete, 2005.

[30] A. Perrot, T. Lecompte, P. Estellé, S. Amziane, Structural build-up of rigid fiber reinforced cement-based materials, Mater. Struct. 46 (2013) 1561–1568. doi:10.1617/s11527-012-9997-9.

[31] F. Mahaut, S. Mokéddem, X. Chateau, N. Roussel, G. Ovarlez, Effect of coarse particle volume fraction on the yield stress and thixotropy of cementitious materials, Cem. Concr. Res. 38 (2008) 1276–1285. doi:10.1016/j.cemconres.2008.06.001

[32] R.J. Farris, Prediction of the Viscosity of Multimodal Suspensions from Unimodal Viscosity Data, J. Rheol. 12 (1968) 281. doi:10.1122/1.549109.

[33] S.D. Jo, C.K. Park, J.H. Jeong, S.H. Lee, S.H. Kwon, A Computational Approach to Estimating a Lubricating Layer in Concrete Pumping, Comput. Mater. Contin. 27 (2012) 189–210. doi:10.3970/cmc.2011.027.189.

[34] M.S. Choi, Y.J. Kim, J.K. Kim, Prediction of Concrete Pumping Using Various Rheological Models, Int. J. Concr. Struct. Mater. 8 (2014). doi:10.1007/s40069-014-0084-1.

[35] Federal Statistical Office, Baugenehmigungen im Hochbau 2014, (2015).

[36] J. Zhang, B. Khoshnevis, Optimal machine operation planning for construction by Contour Crafting, Autom. Constr. 29 (2013) 50–67. doi:10.1016/j.autcon.2012.08.006.

[37] BKI Baukosteninformationszentrum Deutscher Architektenkammern GmbH, Baukosteninformationszentrum Deutscher Architektenkammern, Baukosten Gebäude Neubau 2017 - Statistische Kostenkennwerte, 2015.

[38] Hauptverband der Deutschen Bauindustrie, BGL Baugeräteliste 2015 Technisch-wirtschaftliche Baumaschinendaten, Bauverlag BV GmbH, Gütersloh, 2015.

[39] V.N. Nerella, M. Krause, M. Näther, V. Mechtcherine, Studying printability of fresh concrete for formwork free Concrete on-site 3D Printing technology technology (CONPrint3D), in: Rheol. Messungen an Baustoffen, tredition, Regensburg, 2016: pp. 236–246.

[40] Laura Stampler, Chinese Company WinSun 3D-Printed This 5-Story Apartment Building, (2015). http://time.com/3674557/3d-printed-apartment-building-winsun/ (accessed October 25, 2015).

[41] Cooper Hewitt, Why Design Now?: Contour Crafting - YouTube, (2010). https://www.youtube.com/watch?v=-yv-IWdSdns (accessed March 14, 2016).

[42] Apis-cor, Apis Cor - construction technology, (2017). http://apis-cor.com/en/faq/texnologiya-stroitelstva/ (accessed December 29, 2017).

[43] D. Hwang, B. Khoshnevis, Concrete Wall Fabrication by Contour Crafting, in: ISAR 2004 21st Int. Symp. Autom. Robot. Constr., 2004. doi:10.22260/ISARC2004/0057.

737

738